GEOPHYSICS, VOL. 82, NO. 2 (MARCH-APRIL 2017); P. A 13–A 17, 5 FIGS.
10.1190/GEO2016-0473.1

Directional structure-tensor-based coherence to detect seismic faults and channels

Xinming Wu[1]

ABSTRACT

Seismic coherence is widely used in seismic interpretation and reservoir characterization to highlight (with low values) faults and stratigraphic features from a seismic image. A coherence image can be computed from the eigenvalues of conventional structure tenors, which are outer products of gradients of a seismic image. I have developed a simple but effective method to improve such a coherence image by using directional structure tensors, which are different from the conventional structure tensors in only two aspects. First, instead of using image gradients with vertical and horizontal derivatives, I use directional derivatives, computed in directions perpendicular and parallel to seismic structures (reflectors), to construct directional structure tensors. With these directional derivatives, lateral seismic discontinuities, especially those subtle stratigraphic features aligned within dipping structures, can be better captured in the structure tensors. Second, instead of applying Gaussian smoothing to each element of the constructed structure tensors, I apply approximately fault- and stratigraphy-oriented smoothing to enhance the lateral discontinuities corresponding to faults and stratigraphic features in the structure tensors. Real 3D examples show that the new coherence images computed from such structure tensors display much cleaner and more continuous faults and stratigraphic features compared with those computed from conventional structure tensors and covariance matrices.

INTRODUCTION

Numerous methods, such as crosscorrelation, semblance, eigendecomposition of the covariance matrix, and structure tensor, have been proposed to compute a seismic coherence image (Gersztenkorn and Marfurt, 1999; Chopra and Marfurt, 2007). The crosscorrelation method (Bahorich and Farmer, 1995, 1996) computes seismic coherence using normalized crosscorrelation coefficients of each trace and its inline and crossline neighbors. Semblance was first proposed to compute velocity spectra (Taner and Koehler, 1969; Neidell and Taner, 1971), and then it was further developed as a measure of coherence to detect seismic lateral discontinuities (Marfurt et al., 1998; Hale, 2009). By applying fault-oriented smoothing to the numerators and denominators of semblance ratios, a semblance image can be further enhanced for fault surface extraction (Hale, 2013; Wu and Hale, 2016; Wu et al., 2016). The covariance-matrix-based method (Gersztenkorn and Marfurt, 1999; Marfurt et al., 1999; Li and Lu, 2014) computes seismic coherence using eigenvalues of the covariance matrix constructed from seismic traces. The structure-tensor-based method (Bakker, 2002; Hale, 2009) computes seismic coherence using eigenvalues of structure tensors (Van Vliet and Verbeek, 1995; Weickert, 1997; Fehmers and Höcker, 2003) constructed from gradients of a seismic image. Other methods, such as variance (Van Bemmel and Pepper, 2000; Randen et al., 2001), entropy measurements (Cohen and Coifman, 2002; Cohen et al., 2006), and structural prediction (Karimi et al., 2015), also have been used to compute seismic coherence.

I propose a simple but effective method to improve the structure-tensor-based coherence. In this method, first, I estimate seismic structural and stratigraphic orientations using conventional structure tensors, which are the smoothed outer products of gradients of a seismic image. With the estimated orientations, I compute directional derivatives of the seismic image in directions perpendicular and parallel to the seismic structures. Compared with the gradients with vertical and horizontal derivatives, these directional derivatives can capture more subtle lateral discontinuities aligned within dipping structures. Then, I construct structure tensors using the directional derivatives and applying approximately fault- and stratigraphy-oriented smoothing to each element of the tensors to enhance faults and stratigraphic features in the tensors. Finally, I compute eigendecomposition of the smoothed directional structure tensors and use the eigenvalues to calculate the seismic coherence. Real 3D examples show that the new coherence images display

Manuscript received by the Editor 7 September 2016; revised manuscript received 15 November 2016; published online 17 February 2017.
[1]The University of Texas at Austin, Bureau of Economic Geology, Austin, Texas, USA. E-mail: xinming.wu@beg.utexas.edu.

clean and continuous faults and stratigraphic features, which can be easily tracked.

CONVENTIONAL STRUCTURE TENSORS

Structure tensors, first proposed for common digital image processing (e.g., Kass and Witkin, 1987; Rao and Schunck, 1991; Van Vliet and Verbeek, 1995; Weickert, 1997), have been widely applied to seismic images in estimating the orientations of seismic structural and stratigraphic features and computing the isotropy or anisotropy of the features (Bakker, 2002; Fehmers and Höcker, 2003; Hale, 2009). Structure tensors can be constructed as smoothed outer products of image gradients.

For each sample $\mathbf{x}$ in a 3D seismic image, a structure tensor $\mathbf{T}(\mathbf{x})$ is a 3×3 symmetric positive-semidefinite matrix

$$\mathbf{T} = \langle \mathbf{g}\mathbf{g}^{\mathsf{T}} \rangle = \begin{bmatrix} \langle g_1 g_1 \rangle & \langle g_1 g_2 \rangle & \langle g_1 g_3 \rangle \\ \langle g_1 g_2 \rangle & \langle g_2 g_2 \rangle & \langle g_2 g_3 \rangle \\ \langle g_1 g_3 \rangle & \langle g_2 g_3 \rangle & \langle g_3 g_3 \rangle \end{bmatrix}, \tag{1}$$

where $\mathbf{g} = [\, g_1 \quad g_2 \quad g_3 \,]^{\mathsf{T}}$ is the image gradient vector with first derivatives computed at the image sample $\mathbf{x}$ in the vertical (g_1), inline (g_2), and crossline (g_3) directions. Here, $\langle\cdot\rangle$ denotes smoothing of whatever is inside the angle brackets. This smoothing $\langle\cdot\rangle$, often implemented as a Gaussian filter, is important to obtain stable estimations of seismic structural and stratigraphic orientations. In all examples in this paper, I implement the smoothing $\langle\cdot\rangle$ using a recursive Gaussian smoothing filter (Hale, 2006) with half-widths $\sigma_1 = 6$ (samples), $\sigma_2 = 2$ (samples), and $\sigma_3 = 2$ (samples) in the vertical, inline, and crossline directions, respectively, to construct the conventional structure tensors.

Eigendecomposition

As discussed by Bakker (2002) and Hale (2009), the eigendecomposition of each structure tensor $\mathbf{T}$ can provide estimations of orientation and anisotropy of image features. The eigendecomposition of a 3D structure tensor is as follows:

$$\mathbf{T} = \lambda_u \mathbf{u}\mathbf{u}^{\mathsf{T}} + \lambda_v \mathbf{v}\mathbf{v}^{\mathsf{T}} + \lambda_w \mathbf{w}\mathbf{w}^{\mathsf{T}}, \tag{2}$$

where $\mathbf{u}$, $\mathbf{v}$, and $\mathbf{w}$ are normalized eigenvectors corresponding to the eigenvalues λ_u, λ_v, and λ_w ($\lambda_u \ge \lambda_v \ge \lambda_w \ge 0$), respectively. The eigenvectors $\mathbf{u}$ are perpendicular to locally planar features such as reflectors. The eigenvectors $\mathbf{v}$ and $\mathbf{w}$ are orthogonal to $\mathbf{u}$ and lie within local planes of the reflectors. Moreover, the vectors $\mathbf{v}$ and $\mathbf{w}$ indicate orientations of lateral discontinuities such as faults and stratigraphic features aligned within dipping reflectors (Hale, 2009). Specifically, eigenvectors $\mathbf{w}$ are locally parallel to the fault strikes and stratigraphic features, whereas the eigenvectors $\mathbf{v}$ are orthogonal to them.

Figure 1a shows a 3D synthetic seismic image, in which a horizon surface is picked following the locally planar reflections. This surface is discontinuous at the two faults, and a channel (denoted by cyan arrows) is apparent on the surface. The eigenvectors $\mathbf{v}$ (Figure 1b) and $\mathbf{w}$ (Figure 1c), denoted by the yellow segments, are aligned within the horizon surface. Near the channel and faults, the eigenvectors $\mathbf{v}$ are orthogonal to the channel and the fault strike directions, whereas the eigenvectors $\mathbf{w}$ are locally parallel to both. Away from the channel and faults, $\mathbf{v}$ and $\mathbf{w}$ are arbitrarily oriented but are still aligned within the surface. I compute these vectors for all image samples directly from the seismic image using structure tensors (equation 1) without picking horizon surfaces.

As discussed by Bakker (2002) and Hale (2009), the eigenvalues λ_u, λ_v, and λ_w provide measures of anisotropy such as the planarity and linearity of the image features. In this paper, I define coherence $c(\mathbf{x})$ as a measure of reflector planarity as follows (Hale, 2009):

$$c(\mathbf{x}) = \frac{\lambda_u(\mathbf{x}) - \lambda_v(\mathbf{x})}{\lambda_u(\mathbf{x})}, \tag{3}$$

where we have $0 \le c(\mathbf{x}) \le 1$.

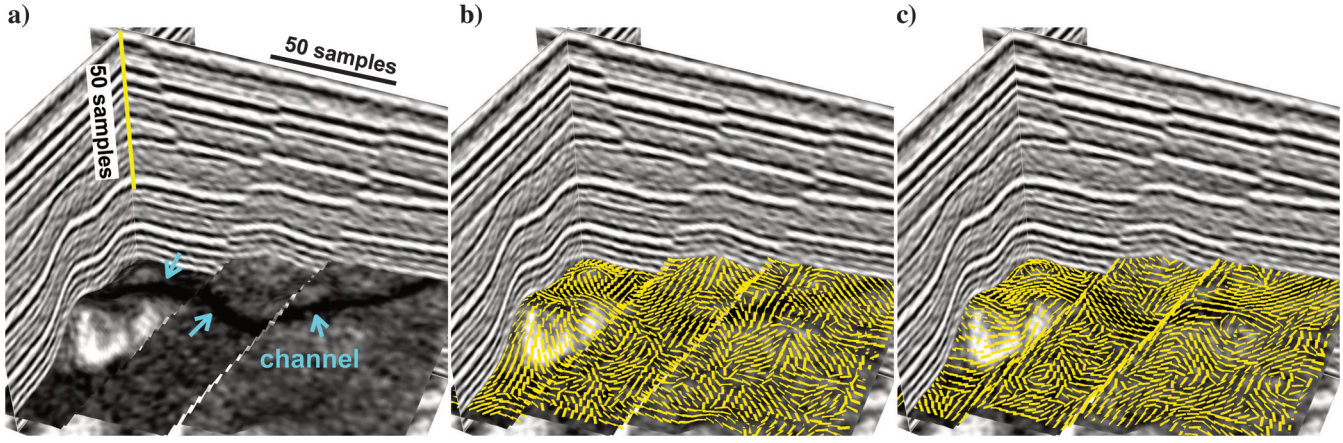

Figure 1. (a) A 3D seismic image is displayed with an interpreted horizon surface. The eigenvectors (yellow segments) (b) $\mathbf{v}$ and (c) $\mathbf{w}$ of the structure tensors are aligned within the horizon surface, and they are perpendicular and parallel to the channel and faults, respectively. These vectors are estimated directly from the seismic image without picking the horizon.

Figure 2a shows a 3D seismic image with channel features apparent on the time slice. To compare with the structure-tensor-based coherence, first, I use the covariance-matrix-based method (Gersztenkorn and Marfurt, 1999; Marfurt et al., 1999) to compute a coherence image (Figure 2b) with nine traces and a vertical window of eight samples for each trace. The vertical window is aligned with seismic reflector dips as discussed by Marfurt et al. (1999). This coherence image highlights (with lower values) most channel features but also noise unrelated to geologic features. The subtle channels denoted by red arrows are visible, but they are not obvious in this coherence image. Figure 3a shows the structure-tensor-based coherence image $c(\mathbf{x})$ (equation 3), which also highlights some stratigraphic features with relatively low values. However, compared with the covariance-matrix-based coherence image (Figure 2b), these features are blurred because of the laterally isotropic smoothing (Gaussian smoothing with half-widths $\sigma_2 = \sigma_3 = 2$ [samples] in the inline and crossline directions) in constructing the structure tensors. In addition, stratigraphic details such as subtle channels (denoted by red arrows) are not resolved in the coherence image because these subtle features are aligned within dipping structures and are not captured in conventional structure tensors constructed with the vertical and horizontal derivatives.

DIRECTIONAL STRUCTURE TENSORS

To resolve subtle stratigraphic features, I propose to construct directional structure tensors using directional derivatives computed in directions perpendicular and parallel to the dipping structures. Also, to enhance faults and stratigraphic features, I apply approximately fault- and stratigraphy-oriented smoothing to each element of the directional structure tensors.

Directional derivatives

Given a 3D seismic image $f(\mathbf{x})$, first, I compute unit eigenvectors $\mathbf{u}(\mathbf{x})$, $\mathbf{v}(\mathbf{x})$, and $\mathbf{w}(\mathbf{x})$ using the conventional structure tensors (equation 1). Then, I compute directional derivatives $g_u(\mathbf{x})$, $g_v(\mathbf{x})$, and $g_w(\mathbf{x})$ as follows:

$$g_u(\mathbf{x}) = \frac{1}{2}[f(\mathbf{x}+\mathbf{u}(\mathbf{x})) - f(\mathbf{x}-\mathbf{u}(\mathbf{x}))],$$
$$g_v(\mathbf{x}) = \frac{1}{2}[f(\mathbf{x}+\mathbf{v}(\mathbf{x})) - f(\mathbf{x}-\mathbf{v}(\mathbf{x}))],$$
$$g_w(\mathbf{x}) = \frac{1}{2}[f(\mathbf{x}+\mathbf{w}(\mathbf{x})) - f(\mathbf{x}-\mathbf{w}(\mathbf{x}))], \quad (4)$$

where I compute $f(\mathbf{x} \pm \mathbf{u}(\mathbf{x}))$, $f(\mathbf{x} \pm \mathbf{v}(\mathbf{x}))$, and $f(\mathbf{x} \pm \mathbf{w}(\mathbf{x}))$ from the seismic image $f(\mathbf{x})$ using the sinc interpolation method. Compared with the simple vertical and horizontal derivatives used in conventional structure tensors (equation 1), these directional derivatives can better capture lateral structure discontinuities, especially those subtle stratigraphic features that are aligned within dipping structures.

Then, I use the directional derivatives to construct directional structure tensors for each image sample $\mathbf{x}$ as

$$\mathbf{T}_s = \begin{bmatrix} \langle g_u g_u \rangle_s & \langle g_u g_v \rangle_s & \langle g_u g_w \rangle_s \\ \langle g_u g_v \rangle_s & \langle g_v g_v \rangle_s & \langle g_v g_w \rangle_s \\ \langle g_u g_w \rangle_s & \langle g_v g_w \rangle_s & \langle g_w g_w \rangle_s \end{bmatrix}, \quad (5)$$

where $\langle \cdot \rangle_s$, again, represents smoothing whatever is inside the brackets.

Smoothing

The smoothing $\langle \cdot \rangle_s$ is not only important to yield stable eigendecompositions of the structure tensors, but it also can be helpful to enhance desired features in the tensors. To preserve and enhance faults and stratigraphic features, I will smooth each element of structure tensors not across, but along such features. This requires the smoothing to be anisotropic, spatially variant, and oriented along the faults and stratigraphic features.

I implement such fault- and stratigraphy-oriented smoothing with anisotropic diffusion (e.g., Weickert, 1997; Fehmers and Höcker, 2003) and implicitly compute the numerical solution of the diffusion by solving the following equation (Hale, 2009):

$$q(\mathbf{x}) - \alpha \nabla \cdot \mathbf{D}(\mathbf{x}) \nabla q(\mathbf{x}) = p(\mathbf{x}). \quad (6)$$

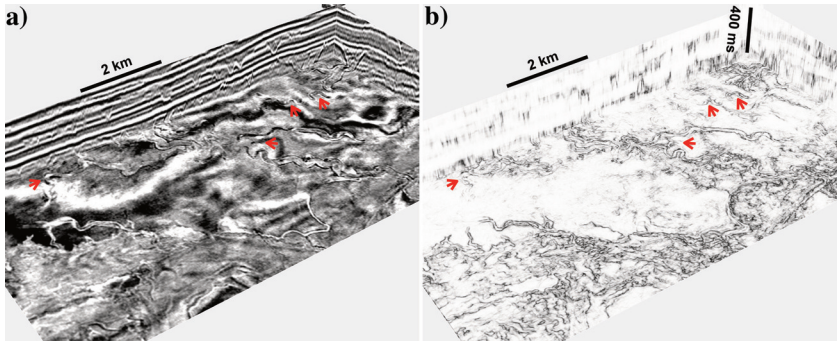

Figure 2. A 3D view of inline, crossline, and time slices of a (a) seismic image and (b) covariance-matrix-based coherence image.

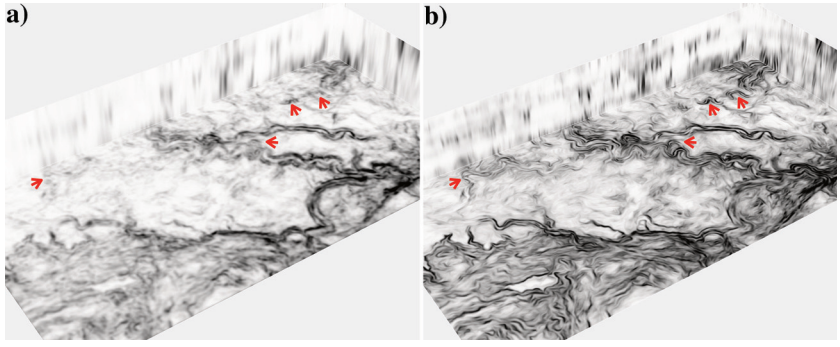

Figure 3. (a) Conventional and (b) directional structure-tensor-based coherence images. The channel features in panel (b) are clearer and more continuous than those in panel (a) and in the covariance-matrix based coherence (Figure 2b). The subtle channels denoted by red arrows in panel (b) are more obvious than in panel (a).

In this equation, $p(\mathbf{x})$ and $q(\mathbf{x})$ represent the input and output images, respectively. The constant parameter α provides a control of the smoothing extent. In all examples in this paper, I used $\alpha = 18$, which corresponds to a smoothing extent approximately comparable with a Gaussian smoothing with a radius $\sigma = 6$ (samples). The diffusion-tensor field $\mathbf{D}(\mathbf{x})$ is important to control the orientations of smoothing. In applications of enhancing seismic reflectors (Fehmers and Höcker, 2003), the diffusion tensor $\mathbf{D}$ for each image sample $\mathbf{x}$ is defined with eigenvectors $\mathbf{v}$ and $\mathbf{w}$ that are locally coplanar to the reflectors: $\mathbf{D} = \mathbf{v}\mathbf{v}^\top + \mathbf{w}\mathbf{w}^\top$.

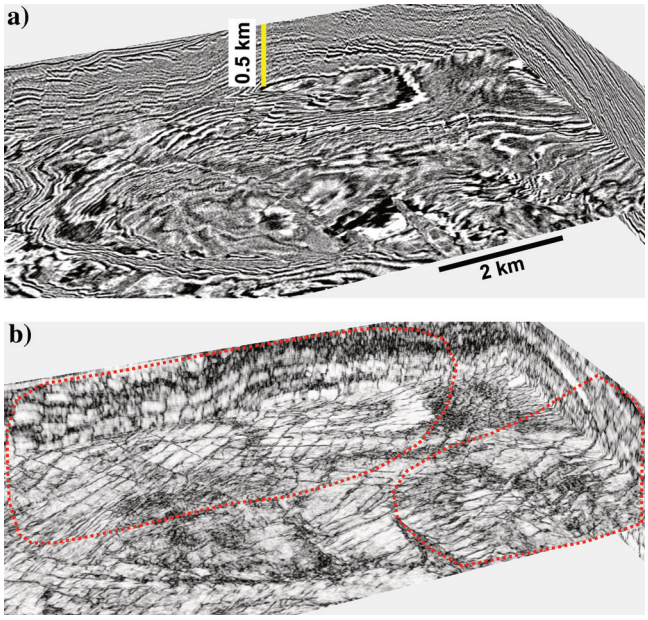

Figure 4. (a) A 3D seismic image and (b) covariance-matrix-based coherence image.

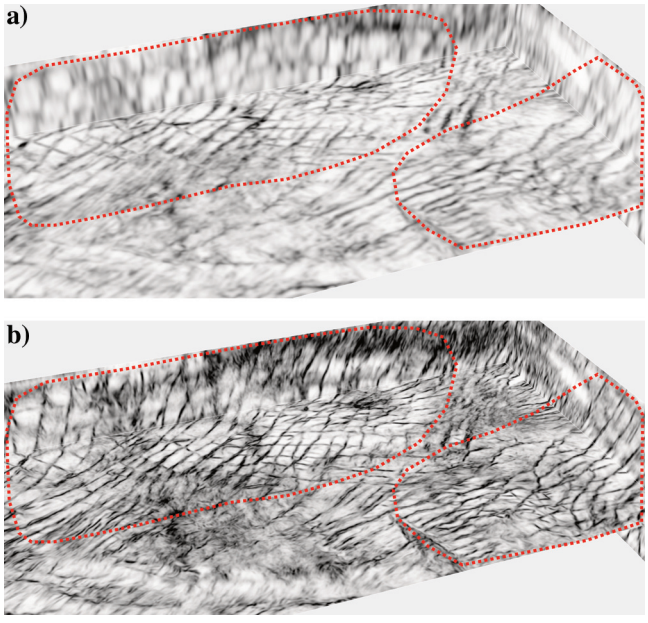

Figure 5. (a) Conventional and (b) directional structure-tensor-based coherence images. In the areas highlighted by dashed red circles, fault features in panel (b) are clearer and more continuous than those in panel (a) and in the covariance-matrix-based coherence (Figure 4b).

However, to enhance faults and stratigraphic features, the diffusion-tensor field should be defined differently. As shown in Figure 1, the eigenvectors $\mathbf{v}$ (Figure 1b) are orthogonal to the channel and fault-strike directions, whereas the eigenvectors $\mathbf{w}$ (Figure 1c) are locally parallel to the channel and fault strikes. Therefore, we should smooth the elements of the structure tensors along vectors $\mathbf{w}$ to laterally enhance faults and stratigraphic features but avoid smoothing along vectors $\mathbf{v}$, which will laterally blur them.

Faults are not only laterally extended in the strike directions, but they also are dipping in some directions. Therefore, in addition to smoothing along the strike directions, we also expect to smooth along the fault-dip directions to enhance faults. It is difficult to estimate fault-dip directions directly from a seismic image, but the eigenvectors $\mathbf{u}$ in many cases can provide reasonable estimations of the fault-dip directions (Bakker, 2002; Hale, 2009). Some large-scale channels may produce incised valleys, which can be significantly large, so that the valley boundaries are visible as lateral reflector discontinuities such as faults in a seismic image. Similarly, the valley boundaries are also likely to be dipping in directions perpendicular to the seismic reflectors. This means that we might also use the eigenvectors $\mathbf{u}$ to approximate the dip directions of the valley boundaries. Therefore, we may also want to smooth along the eigenvectors $\mathbf{u}$ to enhance the channel boundaries and faults.

Based on the discussions above, I implement the anisotropic smoothing $\langle\cdot\rangle_s$ in equation 5 with the diffusion tensor $\mathbf{D}$ as follows to enhance faults and stratigraphic features in structure tensors:

$$\mathbf{D} = \mu_u \mathbf{u}\mathbf{u}^\top + \mu_w \mathbf{w}\mathbf{w}^\top, \tag{7}$$

where the μ_u and μ_w are the constant parameters (between zero and one) used to control the smoothing extents in directions of $\mathbf{u}$ and $\mathbf{w}$. I set $1 \geq \mu_w \geq \mu_u \geq 0$ to enhance stratigraphic features such as channels, which are confirmed to seismic reflections. I set $1 \geq \mu_u \geq \mu_w \geq 0$ to enhance faults, which usually cut through multiple reflections.

After applying the approximately fault- and stratigraphy-oriented smoothing to each element of the directional structure tensors (in equation 5), I again compute the eigendecompositions of the smoothed structure tensors and use the eigenvalues to compute the coherence image as in equation 3. Figure 3b shows a coherence image computed by setting $\mu_u = 0.5$ and $\mu_w = 1$ in constructing the diffusion tensor field (equation 7) for the anisotropic smoothing $\langle\cdot\rangle_s$ in equation 5. Compared with the conventional structure-tensor-based coherence image (Figure 3a), stratigraphic features are enhanced and the subtle channels (denoted by red arrows) are more obvious in this new coherence image (Figure 3b). Compared with this covariance-matrix-based coherence (Figure 2b), the new coherence image (Figure 3b) displays cleaner and more continuous stratigraphic features.

Figure 4a shows another 3D seismic image, from which a covariance-matrix-based coherence image (Figure 4b) is computed with nine traces and a vertical window of 12 samples. Many lateral discontinuities, including faults, are highlighted as relatively low values in this coherence image. However, some of the fault features are noisy and might be difficult to track. Figure 5a shows a conventional structure-tensor-based coherence image, in which the fault

features are blurred compared with the covariance-matrix-based coherence image (Figure 4b). Figure 5b shows a directional structure-tensor-based coherence computed with $\mu_u = 1$ and $\mu_w = 0.5$. In the areas denoted by the dashed red circles, this coherence image displays more continuous and traceable fault features compared with the conventional structure-tensor- (Figure 5a) and the covariance-matrix (Figure 4b)-based coherence images.

CONCLUSION

Two aspects make the directional structure-tensor-based coherence be better than the conventional one to highlight faults and stratigraphic features from a seismic image. First, I construct structure tensors with directional derivatives perpendicular and parallel to seismic reflectors instead of vertical and horizontal derivatives. Second, I smooth each element of the constructed tensors using approximately fault- and stratigraphy-oriented smoothing instead of Gaussian smoothing.

Computing directional structure-tensor-based coherence is more expensive than the conventional one because the anisotropic smoothing for each element of structure tensors is more expensive than Gaussian smoothing. Such anisotropic smoothing is applied three times for constructing 2D structure tensors and six times for 3D ones. With an eight-core computer, my implementation of the method requires approximately 5 and 15 min, respectively, to compute the coherence images in Figures 3b ($140 \times 880 \times 500$ samples) and 5c ($210 \times 920 \times 825$ samples).

In this paper, I used the eigenvectors $\mathbf{u}$ and $\mathbf{w}$ of conventional structure tensors to approximate the fault dip and strike vectors, and I applied smoothing in these dip and strike directions to enhance the faults. The approximations of the fault strikes and dips are reasonable in many cases, but they can be poor for some examples. This indicates that the coherence image can be further improved by using more accurate fault strikes and dips. Such fault strikes and dips might be estimated from a precomputed fault-attribute image.

ACKNOWLEDGMENTS

Thanks go to K. Marfurt, G. Fehmers, and an anonymous reviewer for their valuable suggestions that led to significant improvement of this paper. The seismic image of buried channels is a subset of the Parihaka 3D data set provided by New Zealand Crown Minerals through the SEG Wiki website (http://wiki.seg.org/wiki/Parihaka-3D). The seismic image of faults is a subset of the Costa Rica data set, which is available for academic purposes through the Academic Seismic Portal (http://www.ig.utexas.edu/sdc/). This research is supported by the sponsors of the Texas Consortium for Computational Seismology.

REFERENCES

Bahorich, M., and S. Farmer, 1995, 3D seismic discontinuity for faults and stratigraphic features: The coherence cube: The Leading Edge, **14**, 1053–1058, doi: 10.1190/1.1437077.

Bahorich, M., and S. Farmer, 1996, Method of seismic signal processing and exploration: U.S. Patent US5563949 A.

Bakker, P., 2002, Image structure analysis for seismic interpretation: Ph.D. thesis, Delft University of Technology.

Chopra, S., and K. Marfurt, 2007, Seismic attributes for prospect identification and reservoir characterization: SEG and EAGE.

Cohen, I., and R. R. Coifman, 2002, Local discontinuity measures for 3-D seismic data: Geophysics, **67**, 1933–1945, doi: 10.1190/1.1527094.

Cohen, I., N. Coult, and A. A. Vassiliou, 2006, Detection and extraction of fault surfaces in 3D seismic data: Geophysics, **71**, no. 4, P21–P27, doi: 10.1190/1.2215357.

Fehmers, G. C., and C. F. Höcker, 2003, Fast structural interpretation with structure-oriented filtering: Geophysics, **68**, 1286–1293, doi: 10.1190/1.1598121.

Gersztenkorn, A., and K. J. Marfurt, 1999, Eigenstructure-based coherence computations as an aid to 3-D structural and stratigraphic mapping: Geophysics, **64**, 1468–1479, doi: 10.1190/1.1444651.

Hale, D., 2006, Recursive Gaussian filters: Colorado School of Mines, CWP Report 546.

Hale, D., 2009, Structure-oriented smoothing and semblance: Colorado School of Mines, CWP Report 635.

Hale, D., 2013, Methods to compute fault images, extract fault surfaces, and estimate fault throws from 3D seismic images: Geophysics, **78**, no. 2, O33–O43, doi: 10.1190/geo2012-0331.1.

Karimi, P., S. Fomel, L. Wood, and D. Dunlap, 2015, Predictive coherence: Interpretation, **3**, no. 4, SAE1–SAE7, doi: 10.1190/INT-2015-0030.1.

Kass, M., and A. Witkin, 1987, Analyzing oriented patterns: Computer Vision, Graphics, and Image Processing, **37**, 362–385, doi: 10.1016/0734-189X(87)90043-0.

Li, F., and W. Lu, 2014, Coherence attribute at different spectral scales: Interpretation, **2**, no. 1, SA99–SA106, doi: 10.1190/INT-2013-0089.1.

Marfurt, K. J., R. L. Kirlin, S. L. Farmer, and M. S. Bahorich, 1998, 3-D seismic attributes using a semblance-based coherency algorithm: Geophysics, **63**, 1150–1165, doi: 10.1190/1.1444415.

Marfurt, K. J., V. Sudhaker, A. Gersztenkorn, K. D. Crawford, and S. E. Nissen, 1999, Coherency calculations in the presence of structural dip: Geophysics, **64**, 104–111, doi: 10.1190/1.1444508.

Neidell, N. S., and M. T. Taner, 1971, Semblance and other coherency measures for multichannel data: Geophysics, **36**, 482–497, doi: 10.1190/1.1440186.

Randen, T., S. I. Pedersen, and L. Sønneland, et al., 2001, Automatic extraction of fault surfaces from three-dimensional seismic data: 81st Annual International Meeting, SEG, Expanded Abstracts, 551–554.

Rao, A. R., and B. G. Schunck, 1991, Computing oriented texture fields: CVGIP: Graphical Models and Image Processing, **53**, 157–185, doi: 10.1016/1049-9652(91)90059-S.

Taner, M. T., and F. Koehler, 1969, Velocity spectra-digital computer derivation applications of velocity functions: Geophysics, **34**, 859–881, doi: 10.1190/1.1440058.

Van Bemmel, P. P., and R. E. Pepper, 2000, Seismic signal processing method and apparatus for generating a cube of variance values: U.S. Patent US6151555 A.

Van Vliet, L. J., and P. W. Verbeek, 1995, Estimators for orientation and anisotropy in digitized images: Proceedings of the first annual conference of the Advanced School for Computing and Imaging ASCI'95, 442–450.

Weickert, J., 1997, A review of nonlinear diffusion filtering, *in* B. ter Haar Romeny, L. Florack, J. Koenderink, and M. Viergever, eds., Scale-space theory in computer vision: Springer, doi: 10.1007/3-540-63167-4_37.

Wu, X., and D. Hale, 2016, 3D seismic image processing for faults: Geophysics, **81**, no. 2, IM1–IM11, doi: 10.1190/geo2015-0380.1.

Wu, X., S. Luo, and D. Hale, 2016, Moving faults while unfaulting 3D seismic images: Geophysics, **81**, no. 2, IM25–IM33, doi: 10.1190/geo2015-0381.1.